COMPOSITIONAL DIVERSITY AND STRATIGRAPHIC CHARACTERISTICS OF APOLLO BASIN. Xing Wang[1,2,3], James W. Head[3], Carle M. Pieters[3], Ross W. K. Potter[3,4], Yuan Chen[1], Yuqi Qian[5], Jianjun Liu[1,2], Chunlai Li[1,2], [1]Key Laboratory of Lunar and Deep Space Exploration, National Astronomical Observatories, Chinese Academy of Sciences, Beijing, 100101, China. (wangx01@nao.cas.cn), [2]School of Astronomy and Space Science, University of Chinese Academy of Sciences, Beijing, 100049, China, [3]Department of Earth, Environmental, and Planetary Sciences, Brown University, Providence. 02912, USA [4]Institute for Scientific Information, Clarivate, 70 St Mary Axe, London, EC3A 8BE, UK. [5]Department of Earth Sciences, University of Hong Kong, Hong Kong, China.

Introduction: As the largest impact structure within the South Pole-Aitken (SPA) basin, the 3.98+0.04/-0.06 Ga aged [1] Apollo peak-ring basin may shed significant light on investigating the composition of lunar deep-seated materials, especially given the thin crust nearby (Fig. 1d). The Apollo basin is situated in the interior of the SPA basin from its NE topographic rim toward its interior, implying that in addition to vertical target variation, lateral compositional variation within the SPA basin may be also observed. Numerical modeling suggests that Apollo basin may have formed by impact of a 40 km diameter body traveling at 15 km/s into 20–40 km thick lunar crustal material [2]. Previous studies have noted that, in a manner different from the peak-ring basins outside of SPA, the peak ring of Apollo basin exhibits a more mafic (low-Ca pyroxene, LCP) signature rather than pure anorthosite [3]. The interior of Apollo basin is dominated mainly by noritic materials except the mare region [4] and, similar to elsewhere within the SPA basin, no significant olivine-bearing signature is observed within the Apollo basin [5]. In our research, we conducted a comprehensive analysis of the Apollo basin from additional perspectives (e.g., Th distribution, crustal thickness, etc.) to assess the potential stratigraphy of the Apollo basin and its target.

Compositional diversity within the Apollo basin: We employ Moon Mineralogy Mapper (M^3) data [6] to obtain the spectral features of the Apollo basin. Using the derived band parameters (e.g., band center, BC; band depth, BD) [7], we identify four main material types (Table 1, Fig. 1b). Th distribution and crustal thickness are other critical factors to consider (Fig. 1c, 1d).

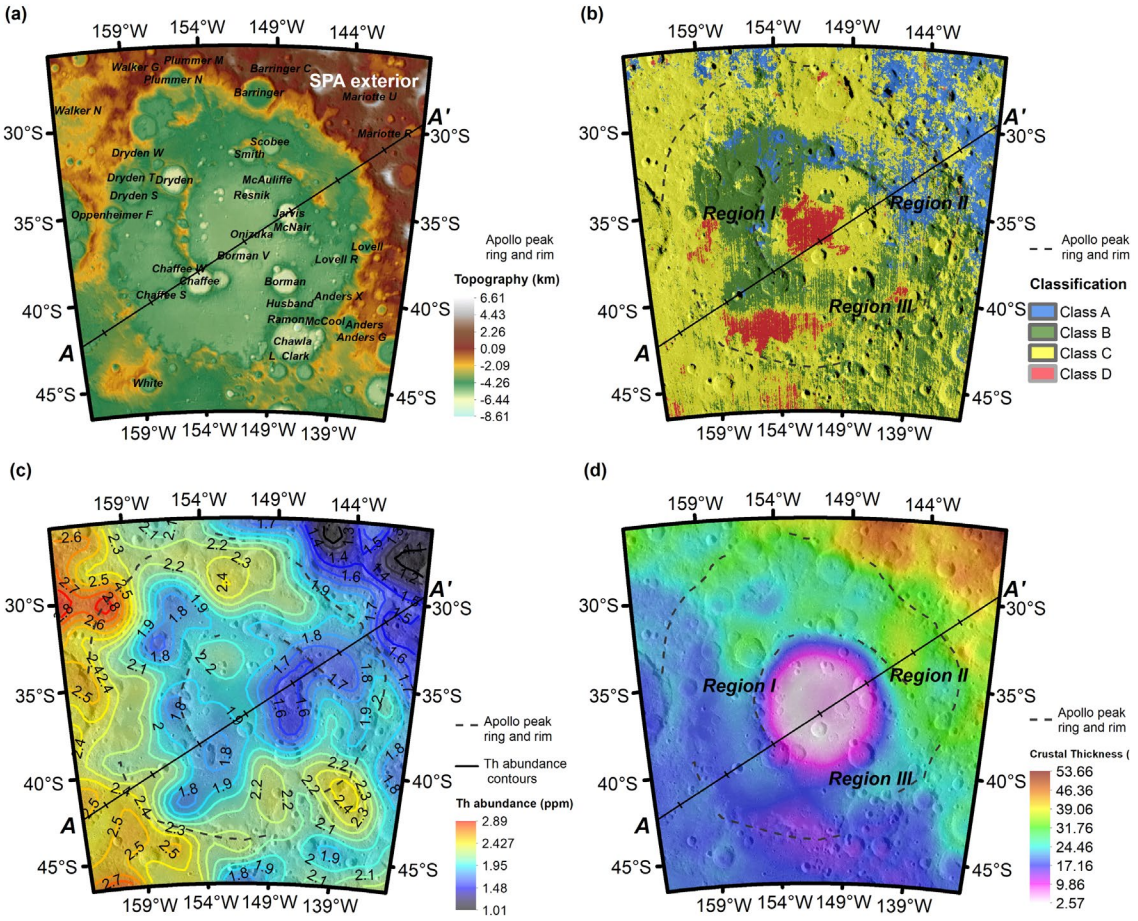

Figure 1. Basic characteristics of Apollo basin. (a) Topographic map from Chang'e-2 DEM data [8]. (b) Spectral features derived from M3 data. (c) Th distribution around Apollo basin from Lunar Prospector Gamma Ray Spectrometer [9]. (d) Crustal Thickness derived from GRAIL (Model 1) [10]. The location of peak ring and rim is from [1].

Table 1. Identifying the materials exposed on the surface of Apollo basin based on band parameters derived from the M³.

Material types	Spectral features	Interpretation
Class A	$BD_{1\mu m}$ < 0.025	feldspathic materials
Class B	$BC_{2\mu m}$ < 2 μm & $BD_{1\mu m}$ > 0.025	Mg-rich noritic materials
Class C	2 μm < $BC_{2\mu m}$ < 2.15 μm & $BD_{1\mu m}$ > 0.025	relatively Fe-rich noritic materials
Class D	$BC_{2\mu m}$ > 2.15 μm	basaltic/gabbro materials

Within the Apollo basin, several interesting features are revealed. For the peak ring, we can observe the same Mg-rich noritic signature ($BC_{2\mu m}$ < 2 μm) as in previous studies, but we also note that the eastern part of the peak ring appears to have higher felspathic abundance. The Th abundance of the entire peak ring region is relatively low (<2 ppm). A large area in the western Apollo interior (Region I) exhibits distinctive Mg-rich noritic features, which are very similar to the materials observed at the peak ring, and local Th abundance is also relatively as low as the peak ring (<2 ppm). However, Region II shows a potentially more feldspathic feature. This feldspathic feature is likely related to the locally elevated crustal thickness (Fig. 1d). In addition, Orientale ejecta (thickness of 0.09~0.22 km estimated by [11]) may also contribute to the feldspathic signature here. Region III in the SE of Apollo interior also shows a possible mixing of the Mg-noritic feature, but with relatively elevated Th abundance. Mare regions show clear HCP-bearing features. Note that the materials of the remaining part of the Apollo interior are also noritic, but they may have slightly higher Ca and Fe contents in their pyroxene composition according to the band center positions (2 μm < $BC_{2\mu m}$ < 2.15 μm). Given that these exposures are pervasive across the entire basin, they could be associated with Apollo impact melt or impact breccia.

Exposure of deep-seated Mg-rich noritic materials: The most distinctive feature discovered in this analysis is the Mg-rich noritic materials appearing in the western and SE portions of the Apollo basin. In the same regions, special microwave thermal emission properties were also found independently by the Chang'E-2 microwave sounder data [12], based on which the existence of these distinct materials is limited in a shallow layer, probably indicating the ejecta deposits excavated by the nearby large impact craters. In addition, the similarity of the exposed components to the peak ring suggests that they may have the same general source. In comparison to the whole SPA basin, their relatively low abundance of Th (<2 ppm) suggests that the source of these materials could be different from that of the materials divided into the Mg-pyroxene annulus in [13], which could be the SPA impact melt or impact breccia (Th abundance >2 ppm) [14]. Following the peak-ring basin formation hypotheses [15], we construct the potential stratigraphy of Apollo basin with the help of these outcrops excavated by the impact craters (Fig. 2).

Considering the deep origin of the peak ring, it is reasonable to speculate that these Mg-rich noritic materials with relatively low Th abundance could be representative of a deep-seated layer (lower crust or mantle) underlying the potential SPA impact breccia. Previous numerical modeling suggests the peak-ring materials could be sourced from lower crust (30-40 km) in the thicker crustal case to up to 70 km in the thinner crustal case, showing a possibility that the Apollo peak ring could originate from the mantle [2]. As the thinner crust was likely on the western side, more Mg-noritic material observation here is consistent with its deeper origin. However, we note that the spectral absorption of the materials exposed in the peak ring is relatively weak, even for the small fresh craters from here. This may imply that the peak ring material could have a relatively high feldspathic abundance (also can be seen from the M3 integrated band depth map in [4]). If the peak ring originates from the mantle, the materials we observed may not match well due to their lower mafic content, but as also mentioned in [16], the peak ring in larger basins may be derived from depths shallower than the maximum depths of excavation. Alternatively, this relatively high feldspathic abundance of the Apollo peak ring may also result from the mixing of crustal and mantle materials during the formation of Apollo basin.

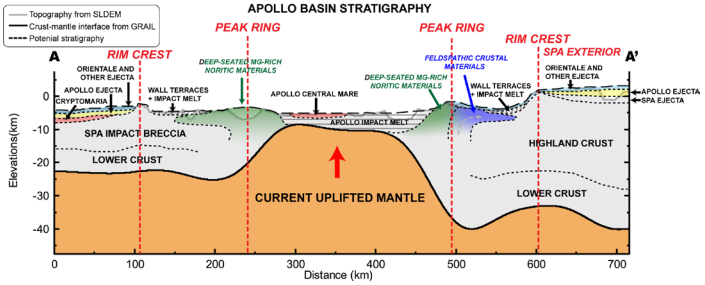

Figure 2. Cross-section of Apollo basin (AA' in Fig.1). Note the topography and crust-mantle interface are the real values derived from SLDEM and GRAIL model 1, respectively, while the dashed lines only show the potential stratigraphy schematically.

Reference:

[1] Ivanov M. A. et al. (2018), *JGR: Planets*, *123(10)*, 2585-2612. [2] Potter, R. W. K. et al. (2018), *Icarus*, *306*, 139-149.[3] Baker, D. M. & Head, J. W. (2015), *Icarus*, *258*, 164-180. [4] Petro, N. E. et al. (2010, March), *LPSC 41*, Abst. #1533. [5] Yamamoto, S. et al. (2012), *Icarus, 218(1)*, 331-344. [6] Pieters, C. M.et al. (2009), *Current Science*, 500-505.6. [7] Liu, D., Wang, X. et al. (2022), *Nat. Commun.*, 13(1), 1-10. [8] Li, C. et al. (2018). *Geomatics Inf. Sci. Wuhan Univ.*, *43(4)*, 485-495. [9] Lawrence, D. J. et al. (2003), *JGR: Planets*, *108(E9)*. [10] Wieczorek, M. A. et al. (2013), *Science*, 339(6120), 671-675. [11] Guo, D. et al. (2018), *JGR: Planets*, *123(6)*, 1344-1367. [12] Meng, Z. et al. (2019), *IEEE J. Sel. Top. Appl. Earth Obs. Remote Sens.*, *12(7)*, 2575-2583. [13] Moriarty, D. P. & Pieters, C. M. (2018), *JGR: Planets*, *123(3)*, 729-747. [14] Moriarty, D. P. et al. (2021), *JGR: Planets*, *126(1)*, e2020JE006589. [15] Baker, D. M. et al. (2016), *Icarus*, *273*, 146-163. [16] Baker, D. M. & Head, J. W. (2015). *Icarus*, *258*, 164-180.